ACSNANO

www.acsnano.org

ARTICLE

Cell to Cell Signaling through Light in Artificial Cell Communities: Glowing Predator Lures Prey

Taniya Chakraborty and Seraphine V. Wegner*

Cite This: *ACS Nano* 2021, 15, 9434–9444

Read Online

ACCESS | Metrics & More | Article Recommendations | Supporting Information

ABSTRACT: Cells commonly communicate with each other through diffusible molecules but nonchemical communication remains elusive. While bioluminescent organisms communicate through light to find prey or attract mates, it is still under debate if signaling through light is possible at the cellular level. Here, we demonstrate that cell to cell signaling through light is possible in artificial cell communities derived from biomimetic vesicles. In our design, artificial sender cells produce an intracellular light signal, which triggers the adhesion to receiver cells. Unlike soluble molecules, the light signal propagates fast, independent of diffusion and without the need for a transporter across membranes. To obtain a predator–prey relationship, the luminescence predator cells is loaded with a secondary diffusible poison, which is transferred to the prey cell upon adhesion and leads to its lysis. This design provides a blueprint for light based intercellular communication, which can be used for programing artificial and natural cell communities.

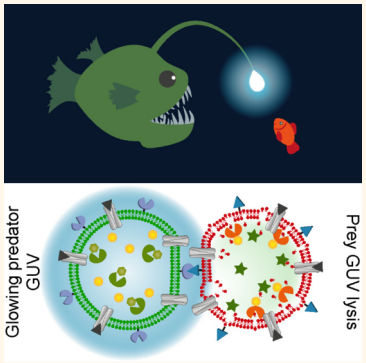

KEYWORDS: *intercellular communication, luminescence, photoswitchable protein, synthetic biology, predator–prey community*

Diffusible signaling molecules are the main basis of intercellular communication.[1,2] This cell-to-cell communication allows cells to adapt functions to their neighbors and can lead to the emergence of collective responses.[3,4] A recent focus in artificial cells is to implement concepts of chemical communication into nonliving systems in order to produce synthetic communities that signal to each other and possess sophisticated behavior.[5−9] Diverse examples of synthetic sender-receiver cells,[6,10,11] bidirectional communication,[12] engineered signaling circuits,[13,14] prey-predator communities,[15−17] communication networks,[18] phagocytosis,[8] and quorum sensing behavior[19−21] demonstrate the versatility of functions that are possible in consortia of synthetic cells using diffusible singling molecules. Building on similar principles, synthetic cells can also be interfaced with living cells and brought together in hybrid communities with enhanced capabilities.[22,23]

Bioluminescence is a widespread signal for the communication between organism at the macroscopic scale, although it is still controversial if plausible at the cellular level.[24,25] From fireflies to deep sea fish, many organisms communicate with others through the light they produce for attracting mates, luring prey, the defense against predators and so on.[26] Light as a specialized mode of communication works particularly well in darkness at night, underground, and in the deep sea and comes with distinct advantages.[27] First, light does not interfere with soluble signaling molecules.[28] Unlike some of the chemical signals such as pH,[29] oxidative species, and metal ions,[30] which alter the activity of many biomolecules, the response to light is rare and highly specific in molecules. Second, visible light passes across optically transparent barriers, such as membranes, and eliminates the need for transporters or pores.[31] In addition, light as a signal is fast in its delivery as it does not require diffusion to propagate. Light is also an information rich signal[24] since different characteristics such as wavelength, brightness, and frequency can code different information. These distinct features of light as a signal make this mode of communication conceptually very attractive.

Here, we present how cell-to-cell communication through light in artificial cell communities is possible. Inspired by deep-sea fish that attract prey through their glow, we implemented this light based mode of communication in synthetic prey–predator communities. We demonstrate that the bioluminescent signal from an artificial predator cell leads to the adhesion to an artificial prey cell. Upon adhesion, the predator injects its

Received: February 22, 2021
Accepted: April 13, 2021
Published: June 21, 2021

https://doi.org/10.1021/acsnano.1c01600
ACS Nano 2021, 15, 9434–9444

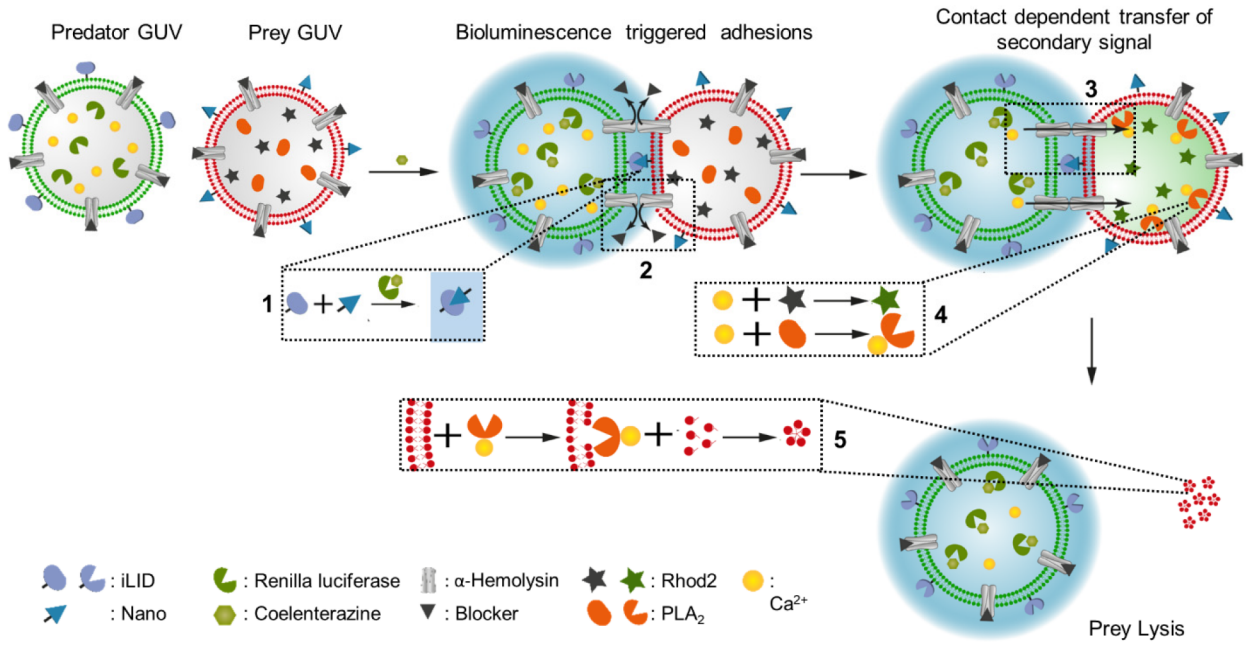

Figure 1. Design of cell to cell communication through light between synthetic predator and prey cells. Predator GUVs are loaded with renilla luciferase and generate an intrinsic light signal upon addition of the substrate coelenterazine. (1) The bioluminescence of the predator GUV, activates the light dependent adhesion of predator (functionalized with iLID, membrane labeled in green) and prey (functionalized with Nano, membrane labeled in red) GUVs, due to the photoswitchable binding of iLID and Nano. (2) The blocker of the α-HL pores is displaced at the adhesion site of the predator and prey GUV and (3) allows for the contact dependent transfer of Ca^{2+}, as a secondary soluble signal, from the predator to the prey GUV. (4) Ca^{2+} binds and activates apo-PLA_2 and the Ca^{2+} sensitive fluorescent dye Rhod2. (5) PLA_2 cleaves the phospholipid membrane of the prey GUV and results in its lysis.

poison into the prey and causes its lysis. This example of communication through light between two synthetic cells demonstrates its plausibility and can serve as a blueprint for the future implementation into living cells and the communication in hybrid systems.

RESULTS AND DISCUSSION

Design of Cell to Cell Communication through Light in a Predator–Prey Community. The generation of an intrinsic light signal and its translation into a response in another cell are the two essential elements for light based communication between cells. The conversion of the intracellular luminescence into an intercellular response requires at least one light responsive element, which is part of a response cascade. In our design, we used luciferase activity to generate the light signal in the sender cell and the photoswitchable protein–protein interaction between iLID and Nano[32−34] as the light responsive element to convey the signal from the sender to the receiver cell. These and many other photoswitchable proteins have been employed in the field of optogenetics for the regulation of diverse functions in cells[35] and synthetic systems[33,34,36,37] with external light sources. More recently, it was shown that bioluminescence can also stimulate some light responsive proteins, which has been used to activate neurons,[38,39] regulate intracellular protein localization[40−42] and trigger bacterial aggregation.[43] In this study, we built on photoactivation with bioluminescence and employed an intrinsically generated light signal in synthetic cells as the basis of intercellular communication.

In particular, we used the bioluminescent signal from one synthetic cell, the sender (the later predator), to activate its adhesion to another cell, the receiver (the later prey) (Figure 1). These cell–cell adhesions were coupled to the exchange of a secondary chemical signal, which in the case predator–prey community functions as a poison and activates the lysis of the prey cell. Throughout the study, we worked with giant unilamellar vesicles (GUVs) as a biomimetic artificial cell model. The predator GUVs contained renilla luciferase (RLuc) inside, such that they generated an intracellular blue light signal in the presence of the substrate, coelenterazine.[44] Coelenterazine is a membrane permeable small molecule and was added externally to initiate the bioluminescence inside the sender GUV. As light responsive elements, the outer membranes of the predator and prey GUVs were decorated with the proteins iLID and Nano, respectively. The two proteins, iLID and Nano, bind to each other under blue light and dissociate in the dark, such that they can mediate adhesions between the GUVs.[34] In this design, we hypothesized that the blue bioluminescence of the luciferase can trigger the adhesion between the two types of GUVs. As part of the response cascade, we implemented adhesion dependent transfer of a secondary soluble molecule from the predator to the prey GUV. For this purpose, the membranes of both the predator and the prey GUVs had incorporated α-hemolysin (α-HL) pores (pore diameter 1.4 nm, MW cutoff = 2000 Da). These pores were blocked with heptakis(2,3,6-tri-*O*-methyl)-*beta*-cyclodextrin (TRIMEB), which noncovalently binds into the lumen of the α-HL pores and prevents the leakage of intracellular content.[11,45] Upon GUV–GUV adhesion, the blocker molecules were excluded from the adhesion sites, as TRIMEB is larger than the intermembrane distance. As a result, otherwise membrane impermeable soluble molecules could pass through the α-HL pores from one GUV to the other. Here in particular, the secondary signal was chosen to be a poison for the receiver GUV so that a predator–prey relationship was established between the two GUV popula-

https://doi.org/10.1021/acsnano.1c01600
ACS Nano 2021, 15, 9434−9444

tions. The predator GUVs were loaded with membrane impermeable Ca^{2+} ions, which upon transfer through the α-HL pores to the prey GUV activate the phospholipase A_2 (PLA_2)[46,47] and lead to a fluorescent signal coming from the calcium sensitive dye, Rhod2. Finally, the calcium activated PLA_2 cleaved the fatty acid tail of the phospholipid in the prey GUVs and caused to their collapse. Toward the realization of this design, we demonstrated step by step each element and finally their integration.

Generation of an Intracellular Light Signal. The first step for the realization of the above envisioned design was the generation of an intracellular light signal and the photoactivation of the iLID protein on the sender GUV though the intracellular bioluminescence. For this purpose, we prepared renilla luciferase (100 nM, RLuc-TEV-His6) loaded GUVs (lipid composition: 1-palmitoyl-2-oleoyl-*sn*-glycero-3-phosphocholine (POPC) with 10 mol % 1-palmitoyl-2-oleoyl-*sn*-glycero-3-phospho-(1′-rac-glycerol) (POPG) + 0.1 mol % DGS-NTA-Ni^{2+}) and immobilized iLID protein at their outer surface through the interaction between the His6-tag on the protein and headgroup of the DGS-NTA-Ni^{2+} lipid. We chose renilla luciferase due to its blue bioluminescence (emission maximum at 482 nm), which has significant spectral overlap with the absorption spectrum of the blue light responsive protein, iLID, around 480 nm (Figure S1a). To generate a bioluminescent signal inside the luciferase loaded GUVs, we added to the external buffer the substrate, coelenterazine (10 μM), which can freely pass across the lipid bilayer without needing a transporter. Indeed, we observed bright bioluminescence from a sample with these GUVs but not in a control sample, which only contained the buffer surrounding the GUVs (Figure 2a). The bioluminescence inside the GUVs had a half-life of 15 min following pseudo first order kinetics and decreased as the substrate was consumed. Moreover, the luminescence could be triggered multiple times upon repeated addition of substrate (Figure S1b). This result showed that an intracellular light signal can be generated in the GUVs upon addition of the substrate, sustained for a considerable duration and even triggered repeatedly.

Intrinsic Luminescence Photoactivates iLID on GUV's Membrane. Next, we investigated if the bioluminescence generated inside the GUVs could activate an extracellular response, *i.e.*, photoactivate iLID and result in the binding to Nano.[48] To address this question, we investigated the recruitment of fluorescently labeled Nano protein without a His-tag, mOrange-Nano (2.5 μM, shown in green), to the above-described luminescent GUVs (100 nM RLuc, iLID protein at the surface, DiD dye in the membrane shown in red) (Figure 2b). We detected a gradual increase in mOrange fluorescence on the GUV membrane upon addition of coelenterazine over the course of 15 min using confocal microscopy (Figure 2c). The quantification of the mOrange fluorescence intensity on the membrane over time showed that the mOrange signal increased for the first 15 min, was stable up to 25 min and later decreased over the course of 60 min to background levels (Figures 2d and S2a). In a negative control without the addition of coelenterazine, no such mOrange-Nano recruitment was observed (Figure S2a). These results demonstrated that the bioluminescence generated inside the GUV activated the iLID protein at the surface, which subsequently lead to the binding of mOrange-Nano. The decrease in iLID-Nano binding was expected at later time points as this binding is reversible in the dark within minutes.[32]

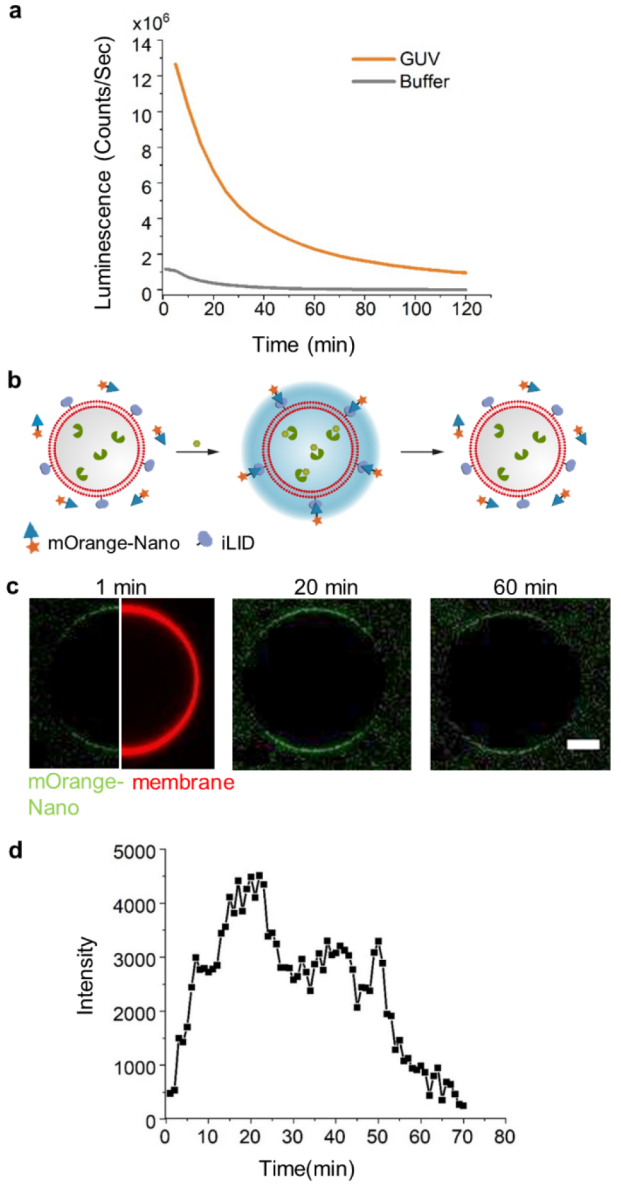

Figure 2. Photoactivation of extracellular iLID and Nano through intracellular bioluminescence. (a) Luminescent of renilla luciferase (100 nM) loaded GUVs(orange) and the external GUV buffer after washing the GUVs (gray, negative control) upon addition of external substrate, coelenterazine (10 μM, orange). The luminescence of the GUVs has a half-life of 15.4 min based on first order kinetic kinetics. (b) Schematic representation of mOrange-Nano protein recruitment due to the bioluminescence of iLID-functionalized GUVs. As the bioluminescence decreases over time mOrange-Nano dissociates from the GUV. (c) Confocal images of an iLID functionalized GUV loaded with renilla luciferase (DiD dye on membrane, shown in red) in the presence of mOrange-Nano (2.5 μM, shown in green) upon addition of coelenterazine (10 μM). Scale bar is 10 μm. (d) Change in mOrange-Nano fluorescence intensity at the GUV membrane over time for the GUV in c. mOrange-Nano was recruited over the first 15 min, remained stable for 50 min and declined to the baseline after 60 min.

As the bioluminescence intensity decreased less iLID protein was photoactivated and the reversion become the dominant reaction.

https://doi.org/10.1021/acsnano.1c01600
ACS Nano 2021, 15, 9434−9444

Cell to Cell Communication through Light Results in Adhesions between Synthetic Cells. Next, we investigated if the intracellular bioluminescence can lead to intercellular communication in the form of adhesions between a sender and a receiver cell.[34]

In this experiment, the sender GUVs were loaded with renilla luciferase (100 nM) and functionalized with iLID at their surfaces and their membranes were labeled with the membrane dye, DiL (shown in green). The receiver GUVs had Nano at their surface (immobilized thought His6-tag on Nano) and were labeled with the membrane dye, DiD (shown in red) (Figure 3a). These two GUV populations were mixed in equivalent ratios in a glass chamber for 30 min with gentle agitation. In one sample, where bioluminescence was triggered through the addition of coelenterazine, the iLID (shown in green) and Nano (shown in red) decorated GUVs adhered to each other as observable with confocal microscopy (Figures 3b and S3a). In comparison, nonluminescent GUVs (*i.e.*, in the absence of coelenterazine) adhered to each other similarly well under blue light (positive control) but didn't adhere to each other in the dark (negative control). The lack of GUV−GUV adhesions in the absence of coelenterazine in dark and the formation of multi-GUV clusters upon addition of the substrate confirmed that the intracellular bioluminescence induced the GUV-GUV adhesions.

The clustering of GUVs upon photoactivation was quantified using automated image analysis and scanning large areas (0.5 mm^2 with *ca.* 300 GUVs) of each sample. In this analysis, the area of each object, including single GUVs and clusters of GUVs, was measured and the average area of all detected objects was used as a metric for clustering: the more the GUVs cluster, the higher was the average area of the detected objects. In this analysis, it was apparent that the average area for GUVs that produced luminescence and that were illumined with blue light was the same and higher than for GUVs kept in the dark (Figure 3c). In parallel, objects with large areas, representing clusters of multiple GUVs, were only observed in the luminescent and the blue light sample but not in the dark (Figure S3b). It should be noted that the total number of sender and receiver GUVs was kept constant between samples to avoid artifacts in clustering arising from overcrowding and difference in confluency (Figure S3c).

The luminescence induced clustering of GUVs was reversible over time as the luminescence decreased (Figures 3d and S4a). More precisely, the GUV clustering was maximal 1 h after inducing the luminescence and decreased significantly after 2 h. In fact, the reversion of the GUV clusters was almost complete after 2 h but still higher than the negative control sample kept in the dark (Figures 3d and S4b,c). As previously shown, not all adhesions between iLID and Nano decorated GUVs were completely reversible as adhesions that strongly deform the GUVs are not reversible.[34]

Coupling Cell to Cell Communication through Light with Contact Dependent Chemicals Communication. In many bioluminescent organisms, the light signal acts as an attractant and once the partner is in close proximity subsequent actions are triggered such as in the mating of fireflies or the luring of a prey in the case of deep sea fish.[25] Inspired by this concept, we designed a predator−prey pair, where the luminescence of the predator GUV first leads to the proximity of the prey GUV followed by the injection of a secondary soluble signal into the prey, which leads to its lysis. This adhesion triggered cell-to-cell communication through

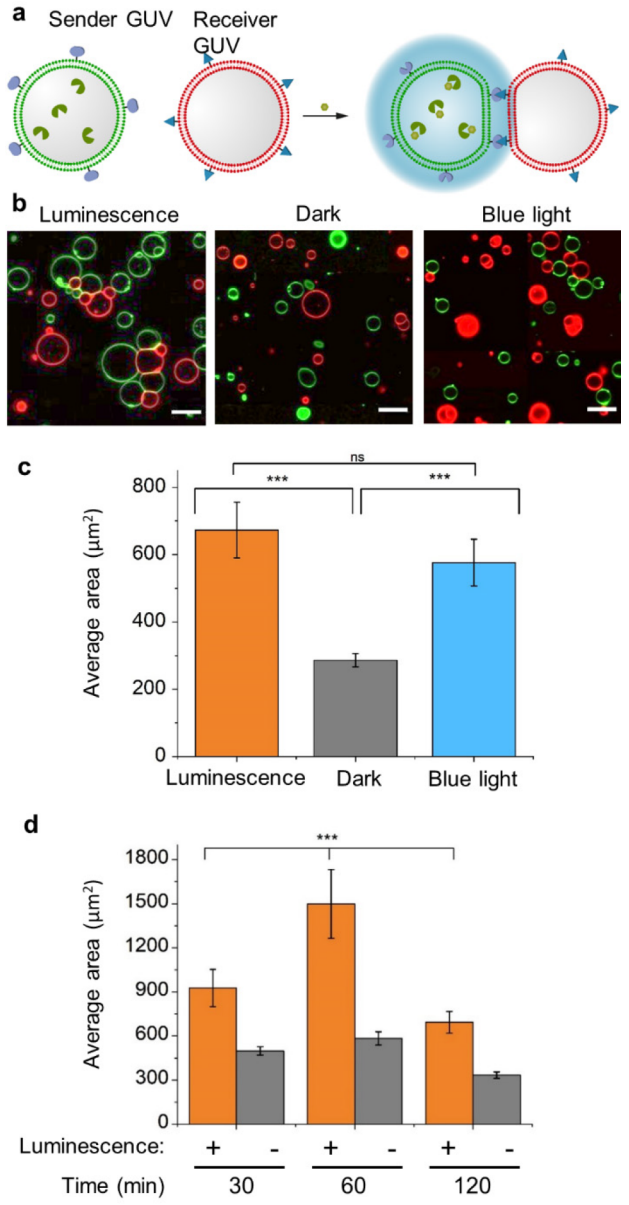

Figure 3. Intrinsic luminescence signal induced adhesion between sender and receiver GUVs. (a) Schematic representation of cell to cell communication through intracellular light. The sender GUV (shown in green) is functionalized with iLID and loaded with renilla luciferase (100 nM), and the receiver GUV (shown in red) is functionalized with Nano. Upon addition of coelenterazine, the sender GUV generates intracellular light, activates iLID on the membrane, which results in the adhesion to the receiver GUV. (b) Confocal images of sender (Dil membrane dye, shown in green) and receiver (DiD membrane dye, shown in red) GUVs in the presence of coelenterazine (10 μM) (luminescence) and in the absence of coelenterazine either in dark (negative control) or under blue light (positive control) after 30 min. Scale bars are 30 μm. (c) Average area of objects (single and clustered GUVs, see Methods for details) described in (b). Sender and receiver GUVs cluster under luminescence as efficiently as under blue light illumination. (d) Average area of objects over time after the addition of coelenterazine to luminescence and dark sample in (b). Luminescence triggered GUV clustering increased over the first 60 min and decreased after 120 min as the luminescence decreased. The average of three technical replicates was reported and statistical significance was evaluated with one-way ANOVA, ***p < 0.001.

https://doi.org/10.1021/acsnano.1c01600
ACS Nano 2021, 15, 9434−9444

secondary soluble signals at the adhesion interphase increases the efficiency of this signal transduction and prevents its loss into the environment through excessive dilution. For this reason, also in biology cell-to-cell communication based on direct contacts are critical in coordinating various processes, from tissue development to immune cell regulation[49] and to the injection of poisons by predator into their prey.

Here, we demonstrated how the luminescence induced adhesions between two populations of GUVs lead to the transfer of a secondary diffusible signaling molecule (Figure 4a). In this case, the above-described sender GUV (loaded with 100 nM RLuc, iLID protein at the surface, DiL dye in the membrane shown in green) were additionally loaded with 2 mM $CaCl_2$ as a secondary signaling molecule. Likewise, the receiver GUVs (Nano protein at the surface, DiD dye in the membrane shown in red) were loaded with the Ca^{2+} sensitive dye, Rhod2 (2 μM, shown in green). Thus, in the here envisioned setup, the transfer of Ca^{2+} from sender to receiver GUVs would be visible as an increase in green Rhod2 fluorescence inside the red labeled receiver GUVs. Unlike the intracellular light signal, Ca^{2+} requires a pore for its transport across the GUV membranes due to its charge, for which we used the transmembrane protein pore α-hemolysin (α-HL, 25 ng/μL). To make the transport of Ca^{2+} adhesion dependent, the α-HL pores were blocked with TRIMEB (4 mM). TRIMEB acts as a blocker of the pores and is removed when two GUV membranes come into proximity such that the transport from one GUV to the next becomes possible at the adhesion interphase through the α-HL pores.

Indeed, when equal numbers of sender and receiver GUVs were mixed an increase of Rhod2 fluorescence was visible in the receiver GUVs upon addition of the coelenterazine using confocal microscopy (Figure 4b). In comparison, a similar increase in Rhod2 fluorescence was also observed in the positive control, where the GUVs adhesions were induced with blue light illumination but not in the negative control, which was kept in the dark and where the GUVs did not adhere to each other. The quantification of the mean fluorescence intensity of Rhod2 inside randomly picked receiver GUVs (n = 30) further supported this observation (Figure 4c). Moreover, both with the bioluminescence and under blue light, the Rhod2 fluorescence only increased in receiver GUVs which were in direct contact with sender GUVs (proximal) but not in receiver GUVs which were far away from sender GUVs (distal). This is further evidence for that the transfer of the Ca^{2+} signal requires the adhesion between sender and receiver GUVs. These results showed that first the luminescence signal from sender GUVs lead to the adhesion of receiver GUVs and subsequently, the transfer of a second soluble Ca^{2+} signal from the sender to the receiver GUVs through the α-HL pore.

Luminescence Induced Prey–Predator Behavior in an Artificial Cell Community. In a population of two different types of artificial cells the transfer of a soluble signaling molecule from one to another can lead to diverse reactions[6,9,22] In particular, we designed a predator–prey couple such that the predator would lure the prey through its bioluminescence and cause its lysis. For this purpose, we employed the above-described Ca^{2+} loaded luminescent sender GUVs as the predator and loaded phospholipase A_2 (PLA_2, 100 nM) enzyme in its apo-form into the receiver GUVs above, which were the prey. The rationale behind this set up was that when the cofactor Ca^{2+} activates apo-PLA_2, it cleaves the fatty acid tail in position two of phospholipids. Thus, the

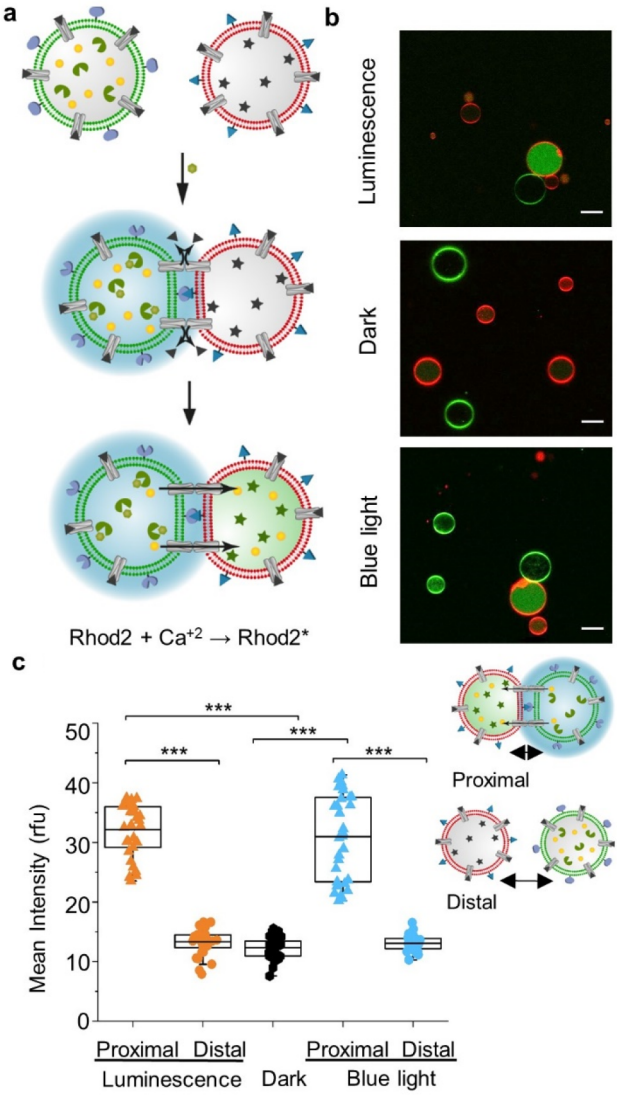

Figure 4. Coupling cell to cell communication through light to contact dependent chemical communication. (a) Schematic representation of contact dependent transfer of a secondary soluble signal following light triggered adhesion. The sender GUV (shown in green) is functionalized with iLID and loaded with renilla luciferase (100 nM) and Ca^{2+} (2 mM) and the receiver GUV (shown in red) is functionalized with Nano and loaded with Rhod2. Both types of GUVs contained α-HL (25 ng/μL), which were blocked by TRIMEB (4 mM). Upon addition of coelenterazine (10 μM), the sender GUV generates intracellular light and activates the adhesion to the receiver GUV. The blocker is displaced at the adhesion interphase and the secondary Ca^{2+} signal is transferred from the sender to the receiver GUV, visible as an increase in fluorescence of Rhod2. (b) Confocal images of sender (Dil membrane dye, shown in green) and receiver (DiD membrane dye, shown in red and intracellular Rhod2, shown in green) GUVs in the presence of coelenterazine (luminescence) and in the absence of coelenterazine either in the dark (negative control) or under blue light (positive control) after 40 min. The intracellular Rhod2 fluorescence increases in the luminescence and the blue light sample, where the sender GUVs adhere to receiver GUVs. Scale bars are 30 μm. (c) Mean Rhod2 fluorescence intensity inside receiver GUVs (n = 30) in (b). In the luminescent and blue light sample, two populations of receiver GUVs were defined as proximal if in close contact with a sender GUV and as distal if not. Statistical significance was evaluated with the one-way ANOVA test, ***p < 0.001.

https://doi.org/10.1021/acsnano.1c01600
ACS Nano 2021, 15, 9434–9444

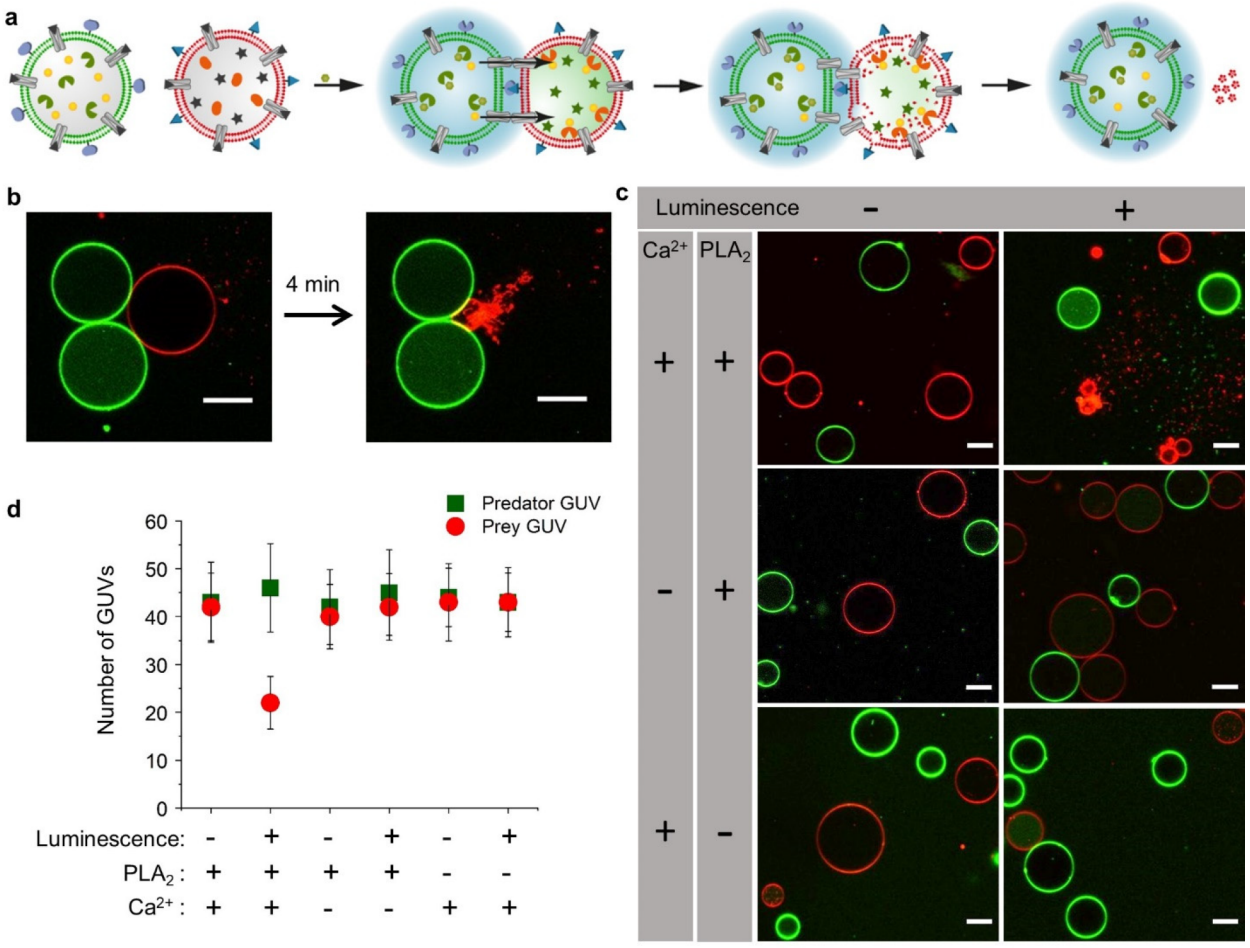

Figure 5. Lysis of prey GUVs by luminescent predator GUVs in a synthetic cell community. (a) Schematic representation of a luminescent predator GUV lysing the prey GUV. The predator GUV (shown in green) is functionalized with iLID and loaded with renilla luciferase (100 nM), Ca^{2+} (2 mM), and the prey GUV (shown in red) is functionalized with Nano and loaded with apo-PLA_2 enzyme and Rhod2. Both types of GUVs contained α-HL (25 ng/μL), which were blocked by TRIMEB (4 mM). Upon addition of coelenterazine (10 μM), the predator GUV generates intracellular light, adheres to the prey GUV, and transfers Ca^{2+} to the prey GUV. Ca^{2+} activates PLA_2, which cleaves the phospholipid bilayer of the prey GUV and results in its lysis. (b) Confocal images of a predator GUV (DiI membrane dye, shown in green), which first adhered to a prey GUV (DiD membrane dye, shown in red) in the presence of coelenterazine and subsequently lysis. See Movie 2. Scale bars are 20 μm. (c) Confocal images of predator and prey GUVs in the absence and presence of coelenterazine after 40 min. Predator GUVs not loaded with Ca^{2+} and prey GUVs not loaded with PLA_2 were used as negative controls. Prey GUVs only lysed when the predator GUV generated intracellular luminescence, contained the secondary Ca^{2+} signal and the prey GUV was loaded with PLA_2. Scale bars are 20 μm. (d) Number of predator or prey GUVs present in (c). The number of prey and predator GUVs was similar in all samples except for the prey GUVs in the presence of coelenterazine, PLA_2 and Ca^{2+}, which was reduced due to their lysis.

Ca^{2+} transferred from predator to the prey GUVs would act as a poison and initiate the digestions of the phospholipid bilayer of prey GUV from inside. Finally, this would result in the lysis of the prey GUV and the formation of micelles (Figure 5a).

In an initial experiment using only prey GUVs, we monitored the lysis of GUVs upon activation of intracellular PLA_2 (100 nM) with externally added Ca^{2+} (1 mM). In this case, the calcium selective ionophore, ionomycin[34] was added to the GUVs to initiate the transfer of the external Ca^{2+} into the GUVs. Indeed, the GUVs lysed a few minutes after the addition of ionomycin, indicating that the Ca^{2+} ions active the PLA_2 enzyme and cleave the phospholipids in the GUV membrane (Figure S5a, Movie 1).

Next, the predator GUVs (100 nM RLuc, 1 mM $CaCl_2$, 25 ng/μL α-HL, iLID protein at the surface, DiL dye in the membrane shown in green) and prey GUVs (100 nM PLA_2, 2 μM Rhod2, 30 μM EDTA, 25 ng/μL α-HL, Nano protein at the surface, DiD dye in the membrane shown in red) were mixed (external buffer: 100 μM EDTA, 4 mM TRIMEB blocker). Then, the bioluminescence inside the predator GUV was triggered through the addition of coelenterazine. In this mixture of prey and predator GUVs, the prey GUVs selectively lysed when the predator GUVs produced light as observed by confocal microscopy (Figures 5b and S5b, Movies S2 and S3). The prey GUV first adhered to predator GUVs within 30 min and then lysed a few minutes later. The lysis of the prey GUV resulted in the formation of small red fluorescent micelles, which were visible in the bulk. In some cases, the prey GUVs lysed, being partially observable as vesicles inside the prey GUVs (Figure S5c,d). On the other hand, prey GUVs did not lyse when no stable contacts formed between prey and predator GUV (Figure S5e, Movie 4). The adhesion dependent transfer of Ca^{2+} ions from the predator to the prey GUV was further supported with similar results when the

https://doi.org/10.1021/acsnano.1c01600
ACS Nano 2021, 15, 9434−9444

adhesions were triggered with blue light illumination rather than luminescence (Figure S5f,g, Movies S5 and S6).

In this predator−prey community, each molecular component in the reaction cascade between the luminescent predator and the prey played an essential role for the final behavior (Figure 5c). The lysis of the prey GUVs was only observed upon triggering the luminescence inside the predator GUVs. On the other hand, the prey and predator GUVs coexisted when the predator GUV was not luminescent. When one of the elements, the primary light signal or the secondary Ca^{2+} signal from the predator or the effector in the prey, PLA_2, was not included in the system, the prey−-predator relationship between the GUVs was impaired. The exclusion of different components stopped the reaction cascade at different stages: the luminescence triggered adhesion between the GUVs in all cases, the exclusion of Ca^{2+} impaired the transfer of the secondary signal and subsequent PLA_2 activation, and the omission of PLA_2 only stopped the lysis of the prey GUVs but the secondary Ca^{2+} was still transferred (visible as an increase in Rhod2 fluorescence in prey GUVs, Figure 5c).

The selective lysis of the prey GUVs was also apparent in the count of the predator (shown in green) and prey (shown in red) GUVs at the population level from the microscopy images (Figure 5d). When the predator GUVs produced light, the number of prey GUVs was reduced by 50% after 40 min. In contrast, without the luminescence of the predator or if the Ca^{2+} in the predator or PLA_2 in the prey GUV were missing, the number of prey GUVs was as high as the predator GUVs, which reflects the initial mixing in equal proportions. This quantification further demonstrated that the activated PLA_2 did not attack the predator GUVs after the lysis of the prey GUVs. There were two reasons behind the predator GUV survival. First, the extracellular EDTA (100 μM) removed the Ca^{2+} ions from PLA_2 once released from the prey GUVs and protects the GUVs from extracellular digestion as GUVs were stable even in the presence of 100 nM PLA_2 with EDTA in the external buffer (Figure 6a). Second, the excessive dilution of PLA_2 in the medium after GUV lysis significantly lowered its activity. Control experiments showed that already a 2-fold dilution of PLA_2 no longer resulted in GUV lysis (Figure S6b). It is noteworthy that it is possible to selectively lyse the prey GUV although the predator and the prey GUVs have the same chemical lipid composition.

CONCLUSIONS

Here, we presented that cell-to-cell communication through light is possible with artificial cells. We have successfully demonstrated that an intrinsic light signal produced in one cell leads to the communication through a molecularly designed reaction cascade. Elements of this reaction cascade are the intracellular bioluminescence of the sender cell, the light triggered adhesion between sender and receiver cells, the adhesion dependent transfer of a coupled secondary signal and response of the receiver cell, which in this case is its lysis. This design is a blue print for the cell-to-cell communication through light and contact dependent exchange of soluble signals as the choice of secondary soluble signals is flexible and can be chosen such that any other desired function is activated.

The communication through light and the coupled downstream activation of follow-up processes is widely spread in biology at the macroscopic scale and should not be underestimated as a mode of communication. Many organisms across the evolutionary tree use bioluminescence to transmit messages and bioluminescence has evolved independently about 40 times, which speaks for its importance. For instance, it is estimated that 90% of deep-sea animals' luminesce[25,26] is used for diverse purposes from mating or prey attraction, protection from predators, to camouflaging. This diversity of functions that built on light based communication calls for translation into synthetic life like systems and speaks for its potential to achieve diverse behavior in consortia of cells.

Whether communication through light is possible between single cells is still controversial.[24] Such communication requires the cells to generate light with some specific property (wavelength, intensity, *etc.*) and another cell to have the ability to sense it. Strong luminescence in the visible range is produced by single cell luminescent bacteria,[19,20] but there is no report that links it to communication with other bacteria. On the other hand, cells emit very weak autoluminescence but it is uncertain if such low photocounts can lead to a cellular reaction. The here presented bioluminescent based signaling between artificial cells shows that indeed communication through light is possible at the cellular level, and this simplified system provides a design model for it. Considering that cells in the human body are not known to bioluminescence, this mode of intercellular communication has the potential to be an orthogonal way to address artificial cells *in vivo*.

The cell-to-cell communication through light has distinct features compared to signaling with diffusible molecules[50,51] in terms of transport across cell boundaries, propagation, and specificity. The transport of soluble signals across a lipid bilayer requires transporters or semipermeable membrane structures,[31] which differ depending on the chemical identity. In contrast, visible light passes through the optically transparent bilayer without the need of further modifications.[52] This difference is also obvious in the here presented example, where the light signal was directly transmitted to the exterior but the secondary Ca^{2+} signal required the presence of α-HL pores. Second, the propagation speed of the signal is limited by diffusion and dilution in the case of chemical signals.[6,10,14,18,34] On the other hand, light signals propagate at the speed of light and are constantly produced at the source as long as the underlying the bioluminescent reaction continues. In the here presented prototype, it was possible to adjust the bioluminescent output and reactivate it as desired, yet for the secondary Ca^{2+} signal it is not possible to replenish it in the sender GUVs once it is released.[11,34] Finally, it should be noted that light as a signal is highly specific as the response of a molecule to visible light is a rather unusual feature and hence undesired cross reactivity is very unlikely. On the other hand, a depending on its chemical identity (acids/bases, metal ions, reactive oxygen species), such a diffusible signal can cause multiple changes in the system. For example, the here used Ca^{2+} signal both activated the PLA_2 and the fluorescence of the dye and in a more complex environment can bind to other proteins and alter their activity.[53]

Opto-chemogenetics, which uses bioluminescence for the activation of optogenetic proteins,[40−42] is a fast-growing part of the optogenetic toolkit as it allows for photoactivation in places that are not accessible to physical light sources.[39] The intrinsic generation of light in the place of interest overcomes limitations in deep tissue penetration of light and its delivery through implanted optical fibers.[54] For instance, opto-chemogenetic systems have made it possible to regulate neuronal activity using light sensitive ion channels with bioluminescence.[38,55] As these approaches gain in importance *in vivo*,

https://doi.org/10.1021/acsnano.1c01600
ACS Nano 2021, 15, 9434−9444

communication through light provides is an orthogonal communication interphase to chemical communication and an opportunity to guide artificial cells in the body.

METHODS

Materials. The Ni^{2+}-NTA functionalized polystyrene beads with a 2 μm diameter were purchased from Micromod Partikeltechnologie GmbH as a water suspension (50 mg/mL, 1.2 × 1010 beads/ml). All lipids, 1-palmitoyl-2-oleoylphosphatidylcholine (16:0−18:1 PC) (catalog number 850457), 1-palmitoyl-2-oleoyl-*sn*-glycero-3-phospho-(1′-rac-glycerol) (16:0−18:1 PG) (catalog number 840457), and 1,2-dioleoyl-*sn*-glycero-3-{(*N*-(5-amino-1-carboxypentyl)-iminodiacetic acid) succinyl} Ni^{2+}-salt (18:1 DGS-NTA(Ni)) (catalog number 790404) were purchased from Avanti Polar Lipids in chloroform. The membrane dyes 1,1′-dioctadecyl-3,3,3′,3′-tetramethylindocarbocyanine perchlorate (DiL) (catalog number D282-100 mg) and 1,1′-dioctadecyl-3,3,3′,3′-Tetramethylindodicarbocyanine (DiD) (catalog number D7757-10 mg) and the calcium sensitive dye Rhod2 (catalogue number R12220) were purchased from Thermo-Fisher Scientific. Coelenterazine native (catalog number 10110) was purchased from Biotium. All others chemicals including α-HL from *Staphylococcus aureus* (catalog number H9395) and TRIMEB (catalog number H4645) were purchased from Sigma-Aldrich. All microscopy experiments for GUV were performed in μ-slide 24-well glass bottom chambers from ibidi (catalogue number 81817).

Plasmids and Proteins. The sequence coding for renilla luciferase was synthesized by the GeneScript and inserted into a pET21b plasmid between the Ndel and Sac1 restriction sites such that it has a TEV cleavable C-terminal His6-tag (RLuc-TEV-His6, Figure S8). pQE-80L iLID (C530M) and pQE-80L MBP-SspB Nano were gifts from Brian Kuhlman (Addgene plasmid # 60408 and 60409, respectively). pQE-80L iLID expresses iLID with an N-terminal His6-tag (His6-iLID), and pQE-80L MBP-SspB Nano expresses Nano with a TEV cleavable N-terminal His6-MBP-tag (His6-MBP-TEV-Nano). The previously described mOrange-Nano plasmid includes an N-terminal TEV cleavable His6-MBP-tag and a mOrange protein fused to the N-terminus of Nano (His6-MBP-TEV-mOrange-Nano). All proteins were expressed and purified as previously described,[48] and details are provided in the Supporting Information.

GUV Preparation, Protein Functionalization, and Washing. GUVs were prepared by the poly(vinyl alcohol) (PVA)-gel assisted formation method and as previously described.[34] In detail, a PVA solution was prepared by mixing 5% (w/v) PVA (MW: 145 000 g/mol) in Milli-Q water with 100 mM sucrose overnight at 400 rpm at 80 °C. A volume of 40 μL of the PVA solution was dried as a thin film on a glass slide (60 mm × 24 mm) at 50 °C for 30 min. Then, 5 μL of a lipid mixture in chloroform containing 10 mol % POPG, 0.1 mol % DGS-NTA-Ni^{2+} and either 0.2 mol % Dil dye or 0.2 mol % DiD dye in 10 mg/mL POPC was spread into the PVA layer and dried for 1 h at 30 °C. Using a Teflon chamber (*ca.* 40 mm × 24 mm) as a spacer and a second glass slide, a chamber was built on top of the slide with PVA and lipid layers. Then, the lipids were hydrated with 1 mL of 100 mM sucrose in Buffer B (10 mM Tris, 100 mM NaCl, pH 7.4) containing all the components to be loaded into the GUV depending on the experiment (100 nM RLuc, 100 nM PLA_2, 30 μM EDTA, 25 ng/μL of α-HL, 1−2 mM $CaCl_2$, 1−2 μM Rhod2) for 1 h at room temperature allowing GUV formation. After that, the chamber was inverted for 5 min, gently taped twice using a pipet tip and the GUVs were harvested into a 1.5 mL LoBind Eppendorf tube.

To functionalize the outer membrane of the GUVs with His-tagged proteins, 400 μL of GUVs was mixed with 1 μM of either His6-tagged iLID or His6-tagged Nano in the dark for 30 min. Next, to wash away excess protein and loaded components, 1 mL of Buffer B supplemented with 100 mM glucose was added to the GUVs and the GUVs were allowed to settle overnight at 4 °C in the dark. The next day morning, the top 1 mL of the buffer was removed without disturbing the bottom layer. The GUVs were washed a second time as before but the GUVs were only allowed to settle for 2 h. In the third washing step, 500 μL of 100 mM glucose containing Buffer B was added and the GUVs were allowed to settle for 1h at room temperature in dark. The bottom 40 μL of each GUV preparation was used in further experiments. In most experiments, 40 μL of iLID and Nano functionalized GUVs were mixed. The three-step washing protocol and the 1:1 mixing of the two GUV types results in a 55-fold dilution (1.8% background) of the GUV loaded components in the exterior buffer, which was used as a negative control in experiments.

For GUVs loaded with α-HL, the buffer contained 4 mM TRIMEB blocker during protein functionalization and all washing steps. For GUVs loaded with PLA_2 the buffer also contained 30 μM EDTA for all steps. For communication and lysis experiments, the GUVs were prepared on the day of the experiment and were allowed to settle for only 2 h in the dark during each washing step.

The partial quenching of mOrange fluorescence by coelenterazine was assessed with GUVs that were functionalized with Histag-mOrange-Nano (Figure S2b).

Luminescence Measurements Inside the GUVs. All luminescence measurements were performed on a multimode plate reader (Spark, Tecan Life Science). GUVs loaded with 100 nM renilla luciferase without membrane dye were prepared and washed as described above. A volume 200 μL of GUVs from the bottom of the tube and exterior buffer from the top of the tube (negative control) were added into 96-well white bottom plate. External coelenterazine (5−20 μM) was added into the solutions just before initiating the luminescence measurements.

mOrange-Nano Recruitment to iLID-GUVs with Bioluminescence. iLID functionalized GUVs loaded with 100 nM RLuc were mixed in a 1:1 ratio with 2.5 μM mOrange-Nano without His-tag in Buffer B in a BSA treated 24-well glass bottom chamber. The GUVs were located under the confocal microscope using the DiD membrane dye (λ_{ex} = 644 nm; λ_{em} = 665 nm) and the recruitment of mOrange-Nano (λ_{ex} = 557 nm; λ_{em} = 576 nm) was triggered through the addition of 10 μM coelenterazine. The mean fluorescence intensity of a whole GUV was quantified using ImageJ and corrected for the background signal.

Luminescence Triggered GUV-GUV Adhesions. The GUV containing tubes were left open for *ca.* 20 min at RT in dark to partially deflate the GUVs. Subsequently, sender GUVs (iLID protein at the surface, DiI membrane dye, loaded with 100 nM RLuc) and receiver GUVs (Nano protein at the surface, DiD membrane dye) were mixed in 1:1 ratio in a BSA coated imaging chamber in the dark. The GUVs mixtures were kept in the dark (negative control) or under blue light (positive control) or in the dark in the presence of 10 μM coelenterazine (luminescent sample). The samples were gently agitated at 30 rpm on an orbital shaker for up to 120 min. Then, a total area of 0.5 mm^2 (737 × 737 μm) was imaged through a 63× water objective in the DiD and DiI channels and analyzed using ImageJ. The images in the DiD and DiI channels were analyzed separately to quantify the number of GUVs of each type and the images in the DiD and DiI channels were merged for the GUV clustering analysis. For both analyses, the images were converted into binary images setting the threshold such that all GUVs were detected, the GUVs were filled with the fill holes function and the number and area of objects larger than 10 μm^2 were detected using the particle analyzer tool. All experiments were performed in triplicate.

Secondary Ca^{2+} Signaling between Sender and Receiver GUVs. Sender GUVs (iLID protein at the surface, DiI membrane dye, loaded with 100 nM RLuc, 2 mM $CaCl_2$ and 25 ng/μL α-HL) and receiver GUVs (Nano protein at the surface, DiD membrane dye, loaded with 2 μM Rhod2 and 25 ng/μL α-HL) were mixed in equal volume in the presence of 4 mM TRIMEB and 30 μM EDTA in a BSA coated imaging chamber and incubated on an orbital shaker at 30 rpm for 40 min. Samples were kept in the dark, under blue light or in the dark in the presence of 10 μM coelenterazine. Images of the GUVs were acquired in the DiI/Rhod2 and DiD channels using confocal microscopy. The mean Rhod2 fluorescence intensity inside randomly picked (n = 30, for each type) receiver GUVs (DiD labeled) proximal and distal to a sender GUV (DiI labeled) was measured using ImageJ.

https://doi.org/10.1021/acsnano.1c01600
ACS Nano 2021, 15, 9434−9444

Lysis of Prey GUVs by Luminescent Predator GUVs. Predator GUVs (iLID protein at the surface, DiI membrane dye, loaded with 100 nM RLuc, 1 mM $CaCl_2$ and 25 ng/μL α-HL) and prey GUVs (Nano protein at the surface, DiD membrane dye, loaded with 100 nM PLA_2, 2 μM Rhod2, 30 μM EDTA and 25 ng/μL α-HL) were mixed in equal volumes in the presence of 4 mM TRIMEB and 100 μM EDTA in a BSA coated imaging chamber and incubated on an orbital shaker at 30 rpm for 40 min in the presence or absence of 10 μM coelenterazine. Similarly, predator GUVs without $CaCl_2$ and prey GUVs without PLA_2 were prepared and mixed with the corresponding prey or predator GUVs in the presence of absence of coelenterazine. Then, images of the GUVs were acquired in the DiD and DiI channels (total area = 0.4 mm^2, 737 μm × 552 μm) and the number of each GUV type as quantified as described above.

Confocal Fluorescence Microscopy. All images were acquired on a Leica SP8 confocal laser scanning microscope through a 63× water objective. The Dil dye and Rhod2 dye were excited with a 552 nm laser, and the emission was detected 560−630 nm (DiI: λ_{ex} = 557 nm; λ_{em} = 576 nm, Rhod2: λ_{ex} = 552 nm; λ_{em} = 581 nm); the DiD dye was excited with a 638 nm laser, and the emission was detected 650−700 nm (DiD: λ_{ex} = 644 nm; λ_{em} = 665 nm). All images were analyzed using ImageJ 1.52b.

Statistical Analysis. The data was presented with the mean ± SEM from three independent samples. The statistical significance was determined by one-way ANOVA using OriginPro9.1. p values: ns > 0.1, *p < 0.1, **p < 0 .01, ***p < 0.001

ASSOCIATED CONTENT

Supporting Information

The Supporting Information is available free of charge at https://pubs.acs.org/doi/10.1021/acsnano.1c01600.

Details of protein purification, absorbance spectrum of iLID and luminescence spectrum of RLuc, additional examples of mOrange-Nano recruitment to luminescent GUVs decorated with iLID, detailed analysis of luminescence induced adhesion and its reversion between iLID and Nano functionalized GUVs, additional examples of predator GUVs lysing prey GUVs including negative controls, SDS-PAGE of proteins, RLuc plasmid map and sequence (PDF)

Receiver GUVs lysis with presence of ionomycin and calcium (AVI)

Prey GUVs lysing after forming adhesions with luminescent predator (AVI)

Prey GUVs lysing after forming adhesions with luminescent predator (AVI)

Prey GUVs not lysing when luminescent predator GUVs pass by without forming adhesions (AVI)

Prey GUVs lysing after forming adhesions with predator GUVs under blue light (AVI)

Prey GUVs lysing after forming adhesions with predator GUVs under blue light (AVI)

AUTHOR INFORMATION

Corresponding Author

Seraphine V. Wegner − *Institute of Physiological Chemistry and Pathobiochemistry, University of Münster, 48149 Münster, Germany; Max Planck Institute for Polymer Research, 55128 Mainz, Germany;* orcid.org/0000-0002-9072-0858; Email: wegnerse@uni-muenster.de

Author

Taniya Chakraborty − *Institute of Physiological Chemistry and Pathobiochemistry, University of Münster, 48149 Münster, Germany; Max Planck Institute for Polymer Research, 55128 Mainz, Germany*

Complete contact information is available at: https://pubs.acs.org/10.1021/acsnano.1c01600

Author Contributions

T.C. and S.V.W. designed the experiments, T.C. conducted the experiments. The manuscript was written through contributions of all authors. All authors have given approval to the final version of the manuscript.

Notes

The authors declare no competing financial interest.

ACKNOWLEDGMENTS

This work is funded by the MaxSynBio consortium, which is jointly funded by the Federal Ministry of Education and Research (BMBF) (FKZ 031A359L) of Germany and the Max Planck Society as well as the Deutsche Forschungsgemeinschaft (DFG, German Research Foundation) − Project-ID 433682494 − SFB 1459. We would like to thank Prof. Brian Kuhlman for the plasmids coding iLID and Nano (Addgene # 60408 and 60409) and Ms. Nina Knubel for technical support with graphic design.

REFERENCES

(1) Aufinger, L.; Simmel, F. C. Establishing Communication between Artificial Cells. *Chem. - Eur. J.* **2019**, *25*, 12659−12670.

(2) Lentini, R.; Martín, N. Y.; Mansy, S. S. Communicating Artificial Cells. *Curr. Opin. Chem. Biol.* **2016**, *34*, 53−61.

(3) Gines, G.; Zadorin, A. S.; Galas, J. C.; Fujii, T.; Estevez-Torres, A.; Rondelez, Y. Microscopic Agents Programmed by DNA Circuits. *Nat. Nanotechnol.* **2017**, *12*, 351−359.

(4) Doğaner, B. A.; Yan, L. K. Q.; Youk, H. Autocrine Signaling and Quorum Sensing: Extreme Ends of a Common Spectrum. *Trends Cell Biol.* **2016**, *26*, 262−271.

(5) Wang, L.; Song, S.; van Hest, J. C. M.; Abdelmohsen, L. K.; Huang, X.; Sánchez, S. Biomimicry of Cellular Motility and Communication Based on Synthetic Soft-Architectures. *Small* **2020**, *16*, 1907680.

(6) Buddingh, B. C.; Elzinga, J.; van Hest, J. C. M. Intercellular Communication between Artificial Cells by Allosteric Amplification of a Molecular Signal. *Nat. Commun.* **2020**, *11*, 1652−1661.

(7) Llopis-Lorente, A.; Díez, P.; Sánchez, A.; Marcos, M. D.; Sancenón, F.; Martínez-Ruiz, P.; Villalonga, R.; Martínez-Máñez, R. Interactive Models of Communication at the Nanoscale Using Nanoparticles That Talk to One Another. *Nat. Commun.* **2017**, *8*, 15511−15517.

(8) Rodriguez-Arco, L.; Kumar, B.; Li, M.; Patil, A. J.; Mann, S. Modulation of Higher-Order Behaviour in Model Protocell Communities by Artificial Phagocytosis. *Angew. Chem., Int. Ed.* **2019**, *58*, 6333−6337.

(9) Li, Q.; Li, S.; Zhang, X.; Xu, W.; Han, X. Programmed Magnetic Manipulation of Vesicles into Spatially Coded Prototissue Architectures Arrays. *Nat. Commun.* **2020**, *11*, 232−240.

(10) Tang, T. D.; Cecchi, D.; Fracasso, G.; Accardi, D.; Coutable-Pennarun, A.; Mansy, S. S.; Perriman, A. W.; Anderson, J. R.; Mann, S. Gene-Mediated Chemical Communication in Synthetic Protocell Communities. *ACS Synth. Biol.* **2018**, *7*, 339−346.

(11) Bolognesi, G.; Friddin, M. S.; Salehi-Reyhani, A.; Barlow, N. E.; Brooks, N. J.; Ces, O.; Elani, Y. Sculpting and Fusing Biomimetic Vesicle Networks Using Optical Tweezers. *Nat. Commun.* **2018**, *9*, 1882−1892.

(12) Joesaar, A.; Yang, S.; Bögels, B.; van der Linden, A.; Pieters, P.; Kumar, B. P.; Dalchau, N.; Phillips, A.; Mann, S.; de Greef, T. F. DNA-Based Communication in Populations of Synthetic Protocells. *Nat. Nanotechnol.* **2019**, *14*, 369−378.

(13) Adamala, K. P.; Martin-Alarcon, D. A.; Guthrie-Honea, K. R.; Boyden, E. S. Engineering Genetic Circuit Interactions within and between Synthetic Minimal Cells. *Nat. Chem.* **2017**, *9*, 431−439.
(14) Dupin, A.; Simmel, F. C. Signalling and Differentiation in Emulsion-Based Multi-Compartmentalized *in vitro* Gene Circuits. *Nat. Chem.* **2019**, *11*, 32−39.
(15) Qiao, Y.; Li, M.; Booth, R.; Mann, S. Predatory Behaviour in Synthetic Protocell Communities. *Nat. Chem.* **2017**, *9*, 110−119.
(16) Balagaddé, F. K.; Song, H.; Ozaki, J.; Collins, C. H.; Barnet, M.; Arnold, F. H.; Quake, S. R.; You, L. A Synthetic *Escherichia coli* Predator-Prey Ecosystem. *Mol. Syst. Biol.* **2008**, *4*, 187−194.
(17) Liu, F.; Mao, J.; Lu, T.; Hua, Q. Synthetic, Context-Dependent Microbial Consortium of Predator and Prey. *ACS Synth. Biol.* **2019**, *8*, 1713−1722.
(18) Yang, S.; Pieters, P. A.; Joesaar, A.; Bögels, B. W.; Brouwers, R.; Myrgorodska, I.; Mann, S.; de Greef, T. F. Light-Activated Signaling in DNA-Encoded Sender-Receiver Architectures. *ACS Nano* **2020**, *14*, 15992−16002.
(19) Niederholtmeyer, H.; Chaggan, C.; Devaraj, N. K. Communication and Quorum Sensing in Non-Living Mimics of Eukaryotic Cells. *Nat. Commun.* **2018**, *9*, 5027−5034.
(20) Gardner, P. M.; Winzer, K.; Davis, B. G. Sugar Synthesis in a Protocellular Model Leads to a Cell Signalling Response in Bacteria. *Nat. Chem.* **2009**, *1*, 377−383.
(21) Liu, Y.; Wu, H. C.; Chhuan, M.; Terrell, J. L.; Tsao, C. Y.; Bentley, W. E.; Payne, G. F. Functionalizing Soft Matter for Molecular Communication. *ACS Biomater. Sci. Eng.* **2015**, *1*, 320−328.
(22) Li, S.; Wang, X.; Mu, W.; Han, X. Chemical Signal Communication between Two Protoorganelles in a Lipid-Based Artificial Cell. *Anal. Chem.* **2019**, *91*, 6859−6864.
(23) Wang, X.; Tian, L.; Du, H.; Li, M.; Mu, W.; Drinkwater, B. W.; Han, X.; Mann, S. Chemical Communication in Spatially Organized Protocell Colonies and Protocell/Living Cell Micro-Arrays. *Chem. Sci.* **2019**, *10*, 9446−9453.
(24) Kučera, O.; Cifra, M. Cell-to-Cell Signaling through Light: Just a Ghost of Chance? *Cell Commun. Signaling* **2013**, *11*, 87−94.
(25) Martini, S.; Haddock, S. H. Quantification of Bioluminescence from the Surface to the Deep Sea Demonstrates Its Predominance as an Ecological Trait. *Sci. Rep.* **2017**, *7*, 45750−45760.
(26) Burford, B. P.; Robison, B. H. Bioluminescent Backlighting Illuminates the Complex Visual Signals of a Social Squid in the Deep Sea. *Proc. Natl. Acad. Sci. U. S. A.* **2020**, *117*, 8524−8531.
(27) Widder, E. A. Bioluminescence in the Ocean: Origins of Biological, Chemical and Ecological Diversity. *Science* **2010**, *328*, 704−708.
(28) Laager, F. Light Based Cellular Interactions: Hypotheses and Perspectives. *Front. Phys.* **2015**, *3*, 55.
(29) Ghazvini, S.; Alonso, R.; Alhakamy, N.; Dhar, P. pH-Induced Changes in the Surface Viscosity of Unsaturated Phospholipids Monitored Using Active Interfacial Microrheology. *Langmuir* **2018**, *34*, 1159−1170.
(30) Valko, M.; Morris, H.; Cronin, M. T. D. Metals, Toxicity and Oxidative Stress. *Curr. Med. Chem.* **2005**, *12*, 1161−1208.
(31) Vanuytsel, S.; Carniello, J.; Wallace, M. I. Artificial Signal Transduction across Membranes. *ChemBioChem* **2019**, *20*, 2569−2580.
(32) Guntas, G.; Hallett, R. A.; Zimmerman, S. P.; Williams, T.; Yumerefendi, H.; Bear, J. E.; Kuhlman, B. Engineering an Improved Light-Induced Dimer (iLID) for Controlling the Localization and Activity of Signaling Proteins. *Proc. Natl. Acad. Sci. U. S. A.* **2015**, *112*, 112−117.
(33) Chervyachkova, E.; Wegner, S. V. Reversible Social Self-Sorting of Colloidal Cell-Mimics with Blue Light Switchable Proteins. *ACS Synth. Biol.* **2018**, *7*, 1817−1824.
(34) Chakraborty, T.; Bartelt, S. M.; Steinkühler, J.; Dimova, R.; Wegner, S. V. Light Controlled Cell-to-Cell Adhesion and Chemical Communication in Minimal Synthetic Cells. *Chem. Commun.* **2019**, *55*, 9448−9451.
(35) Mueller, M.; Rasoulinejad, S.; Garg, S.; Wegner, S. V. The Importance of Cell-Cell Interaction Dynamics in Bottom-Up Tissue Engineering: Concepts of Colloidal Self-Assembly in the Fabrication of Multicellular Architectures. *Nano Lett.* **2020**, *20*, 2257−2263.
(36) Senturk, O. I.; Chervyachkova, E.; Ji, Y.; Wegner, S. V. Independent Blue and Red Light Triggered Narcissistic Self-Sorting Self-Assembly of Colloidal Particles. *Small* **2019**, *15*, 1901801.
(37) Bartelt, S. M.; Steinkühler, J.; Dimova, R.; Wegner, S. V. Light-Guided Motility of a Minimal Synthetic Cell. *Nano Lett.* **2018**, *18*, 7268−7274.
(38) Berglund, K.; Tung, J. K.; Higashikubo, B.; Gross, R. E.; Moore, C. I.; Hochgeschwender, U. Combined Optogenetic and Chemogenetic Control of Neurons. *Methods Mol. Biol.* **2016**, *1408*, 207−225.
(39) Berglund, K.; Clissold, K.; Li, H. E.; Wen, L.; Park, S. Y.; Gleixner, J.; Klein, M. E.; Lu, D.; Barter, J. W.; Rossi, M. A.; Augustine, G. J.; Yin, H. H.; Hochgeschwender, U. Luminopsins Integrate Opto- and Chemogenetics by Using Physical and Biological Light Sources for Opsin Activation. *Proc. Natl. Acad. Sci. U. S. A.* **2016**, *113*, E358−E367.
(40) Kim, C. K.; Cho, K. F.; Kim, M. W.; Ting, A. Y. Luciferase-LOV BRET Enables Versatile and Specific Transcriptional Readout of Cellular Protein-Protein Interactions. *eLife* **2019**, *8*, 43826−43846.
(41) Salinas, F.; Rojas, V.; Delgado, V.; López, J.; Agosin, E.; Larrondo, L. F. Fungal Light-Oxygen-Voltage Domains for Optogenetic Control of Gene Expression and Flocculation in Yeast. *mBio* **2018**, *9*, No. e00626-18.
(42) Parag-Sharma, K.; O'Banion, C. P.; Henry, E. C.; Musicant, A. M.; Cleveland, J. L.; Lawrence, D. S.; Amelio, A. L. Engineered BRET-Based Biologic Light Sources Enable Spatiotemporal Control Over Diverse Optogenetic Systems. *ACS Synth. Biol.* **2020**, *9*, 1−9.
(43) Chen, F.; Warnock, R. L.; Van der Meer, J. R.; Wegner, S. V. Bioluminescence-Triggered Photoswitchable Bacterial Adhesions Enable Higher Sensitivity and Dual-Readout Bacterial Biosensors for Mercury. *ACS Sens.* **2020**, *5*, 2205−2210.
(44) Woo, J.; von Arnim, A. G Mutational Optimization of the Coelenterazine-Dependent Luciferase from Renilla. *Plant Methods* **2008**, *4*, 23−33.
(45) Thomas, J. M.; Friddin, M. S.; Ces, O.; Elani, Y. Programming Membrane Permeability Using Integrated Membrane Pores and Blockers as Molecular Regulators. *Chem. Commun.* **2017**, *53*, 12282−12285.
(46) Vacklin, H. P.; Tiberg, F.; Fragneto, G.; Thomas, R. K. Phospholipase A_2 Hydrolysis of Supported Phospholipid Bilayers: A Neutron Reflectivity and Ellipsometry Study. *Biochemistry* **2005**, *44*, 2811−2821.
(47) Kai, S.; Li, X.; Li, B.; Han, X.; Lu, X. Calcium-Dependent Hydrolysis of Supported Planar Lipids was Triggered by Honey Bee Venom Phospholipase A2 with the Right Orientation at the Interface. *Phys. Chem. Chem. Phys.* **2018**, *20*, 63−67.
(48) Bartelt, S. M.; Chervyachkova, E.; Steinkühler, J.; Ricken, J.; Wieneke, R.; Tampe, R.; Dimova, R.; Wegner, S. V. Dynamic Blue Light-Switchable Protein Patterns on Giant Unilamellar Vesicles. *Chem. Commun.* **2018**, *54*, 948−951.
(49) Daneshpour, H.; Youk, H. Modeling Cell-Cell Communication for Immune Systems across Space and Time. *Curr. Opin. Syst. Biol.* **2019**, *18*, 44−52.
(50) Hindley, J. W.; Zheleva, D. G.; Elani, Y.; Charalambous, K.; Barter, L. M.; Booth, P. J.; Bevan, C. L.; Law, R. V.; Ces, O. Building a Synthetic Mechanosensitive Signaling Pathway in Compartmentalized Artificial Cells. *Proc. Natl. Acad. Sci. U. S. A.* **2019**, *116*, 16711−16716.
(51) Peng, R.; Xu, L.; Wang, H.; Lyu, Y.; Wang, D.; Bi, C.; Cui, C.; Fan, C.; Liu, Q.; Zhang, X.; Tan, W. DNA-Based Artificial Molecular Signaling System That Mimics Basic Elements of Reception and Response. *Nat. Commun.* **2020**, *11*, 978−987.
(52) Glantz, S. T.; Berlew, E. E.; Jaber, Z.; Schuster, B. S.; Gardner, K. H.; Chow, B. Y. Directly Light-Regulated Binding of RGS-LOV Photoreceptors to Anionic Membrane Phospholipids. *Proc. Natl. Acad. Sci. U. S. A.* **2018**, *115*, E7720−E7727.

https://doi.org/10.1021/acsnano.1c01600
ACS Nano 2021, 15, 9434−9444

(53) Charalambous, K.; Booth, P. J.; Woscholski, R.; Seddon, J. M.; Templer, R. H.; Law, R. V.; Barter, L. M.; Ces, O. Engineering *de Novo* Membrane-Mediated Protein-Protein Communication Networks. *J. Am. Chem. Soc.* **2012**, *134*, 5746−5749.
(54) Birkner, E.; Berglund, K.; Klein, M. E.; Augustine, G. J.; Hochgeschwender, U. Non-Invasive Activation of Optogenetic Actuators. *Proc. SPIE* **2014**, *8928*, 89282F.
(55) Kuchimaru, T.; Iwano, S.; Kiyama, M.; Mitsumata, S.; Kadonosono, T.; Niwa, H.; Maki, S.; Kizaka-Kondoh, S. A Luciferin Analogue Generating Near-Infrared Bioluminescence Achieves Highly Sensitive Deep-Tissue Imaging. *Nat. Commun.* **2016**, *7*, 11856−11863.

https://doi.org/10.1021/acsnano.1c01600
ACS Nano 2021, 15, 9434−9444